Electrocatalysis

Deutsche Ausgabe: DOI: 10.1002/ange.201602888
Internationale Ausgabe: DOI: 10.1002/anie.201602888

# Highly Efficient, Selective, and Stable $CO_2$ Electroreduction on a Hexagonal Zn Catalyst

*Da Hye Won, Hyeyoung Shin, Jaekang Koh, Jaehoon Chung, Hee Sang Lee, Hyungjun Kim,* and Seong Ihl Woo**

***Abstract:*** *Electrocatalytic $CO_2$ conversion into fuel is a prospective strategy for the sustainable energy production. However, still many parts of the catalyst such as low catalytic activity, selectivity, and stability are challenging. Herein, a hierarchical hexagonal Zn catalyst showed highly efficient and, more importantly, stable performance as an electrocatalyst for selectively producing CO. Moreover, we found that its high selectivity for CO is attributed to morphology. In electrochemical analysis, Zn (101) facet is favorable to CO formation whereas Zn (002) facet favors the $H_2$ evolution during $CO_2$ electrolysis. Indeed, DFT calculations showed that (101) facet lowers a reduction potential for $CO_2$ to CO by more effectively stabilizing a *COOH intermediate than (002) facet. This further suggests that tuning the crystal structure to control (101)/(002) facet ratio of Zn can be considered as a key design principle to achieve a desirable product from Zn catalyst.*

Electrochemical $CO_2$ conversion into fuel coupling with renewable electricity is a promising strategy to alleviate anthropogenic climate change and depletion of fossil fuel.[1] As $CO_2$ reduction involves sluggish kinetics, the success in this system requires the development of catalyst with good catalytic activity, selectivity and stability. Among various metal candidates that have been extensively investigated since the early 1990s, noble metals (e.g., Ag[2] and Au[3]) have attracted much attention due to their selective production of CO, which can be used for producing higher-energy density fuels with $H_2$. For the practical application, however, it is also required to develop low-cost and earth-abundant metal catalyst. In that sense, non-noble metal Zn is one of the promising materials because of its abundant reserves and particularly selective production of CO.[4] To develop Zn metal as an electrocatalyst, the first priority is not only an enhancement of the catalytic activity towards $CO_2$ reduction, but also a prolongation of the catalyst durability.

Several studies have focused on the modulation of morphology to enhance the catalytic performance compared to bulk metal electrodes.[2c,d,3b–e,4a,5] Moreover, manipulating the structure of catalyst could control the product selectivity by introducing local active sites as well as increase the current density.[3b–e,5c–g] Indeed, the effect of morphology on catalytic selectivity has been experimentally and computationally investigated for metal catalysts such as Au,[3c] Cu,[5a–d] and Pd.[5g] However, in case of Zn, only a few studies report its catalytic activity for $CO_2$ reduction by using the structure modified catalysts such as Zn dendrite[4a] and nanoscale Zn catalyst[4b] and the factor to govern entire catalysis on Zn electrode still remain unknown because of the lack of mechanistic understanding.

Another crucial factor of catalyst performance is a stable long-term operation, which is one of the essentials for commercial application. Despite its significance, the catalyst durability has not yet been extensively evaluated or discussed in previous reports. Although the use of noble metal catalysts cannot guarantee the long-term stability of $CO_2$ conversion, one should be even more cautious about the catalyst stability when using vulnerable non-noble metals such as Zn. In previous studies on Zn-based electrodes, for example, Zn dendrite and nanoscale Zn catalysts, their performances were evaluated only for 3 and 10 h, respectively.[4a,b] To our knowledge, even in cases of novel metal based electrodes selectively producing CO, the reported operating time without significant performance degradation is not exceeded over half a day.[2a,3c–e] Therefore, the performance profile during long-time operation more than a day needs to be examined and it should be improved for further advance of $CO_2$ reduction process.

In this work, we developed a hierarchical hexagonal Zn catalyst (*h*-Zn) for highly active $CO_2$ reduction reaction. The unprecedented operation time (ca. 30 h) and high selectivity (ca. 95%) for CO production were achieved as well as a superior CO production rate. Furthermore, the origin of catalytic selectivity derived from the Zn structure was theoretically analyzed by density functional theory (DFT) calculations.

The *h*-Zn electrode was simply prepared by electrodeposition of $ZnCl_2$ on a Zn foil. The morphology of the *h*-Zn was observed with field emission scanning electron microscopy (FESEM). As shown in Figure 1, the hexagonal shape of Zn pieces was densely aligned on the fabricated electrode. The Zn pieces were ranged from about 400 nm to 1.5 μm and arranged with various directions. Because of the continuous formation of Zn networks, the unique rough structure was constructed (see Figure S1 in the Supporting Information)

[*] D. H. Won, J. Chung, H. S. Lee, Prof. S. I. Woo
Department of Chemical and Biomolecular Engineering
Korea Advanced Institute of Science and Technology
Daejeon 34141 (Republic of Korea)
E-mail: siwoo@kaist.ac.kr
H. Shin, J. Koh, Prof. H. Kim
Graduate School of Energy, Environment, Water and Sustainability (EEWS)
Korea Advanced Institute of Science and Technology
Daejeon 34141 (Republic of Korea)
E-mail: linus16@kaist.ac.kr

Supporting information for this article can be found under: http://dx.doi.org/10.1002/anie.201602888.

  

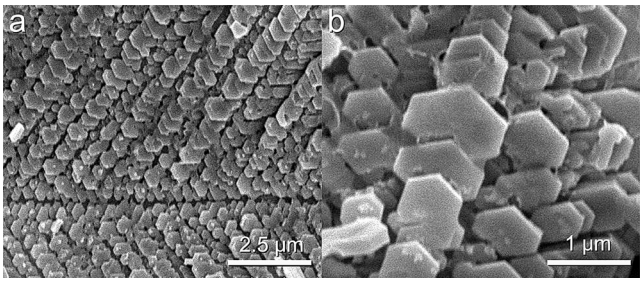


***Figure 1.*** Surface morphology of the prepared *h*-Zn observed by FESEM.

and the enhanced surface area was also confirmed by an increased double layer capacitance compared to the pristine Zn foil (Figure S2). The crystal structure of the *h*-Zn analyzed by a thin-film X-ray diffraction (XRD) pattern was well matched to pure-metallic Zn (Figure S3a). In X-ray photoelectron spectroscopy Zn 2p analysis, however, the surface of the *h*-Zn was composed of $Zn^{II}$ state as well as metallic Zn because the oxidation of Zn metal is highly spontaneous reaction in presence of air and moisture (Figure S3b). The surface oxidation phenomenon was also identified on the pristine Zn foil (Figure S3c). According to the previous studies, the existence of native oxide layer might have an positive effect to $CO_2$ reduction by stabilization of reaction intermediate.[3e,5e,h] Nevertheless, the role of native oxide layer would not be a significant distraction factor for comparing the catalytic performance of the prepared Zn electrodes in this study because all Zn electrodes possessed native oxide layer.

All the prepared Zn electrodes were pretreated by cyclic voltammetry to reduce the oxide layer before every electrochemical investigation (Figure S4). The electrochemical activity of the prepared Zn electrodes was evaluated by linear sweep voltammetry (LSV) to determine the catalytic ability

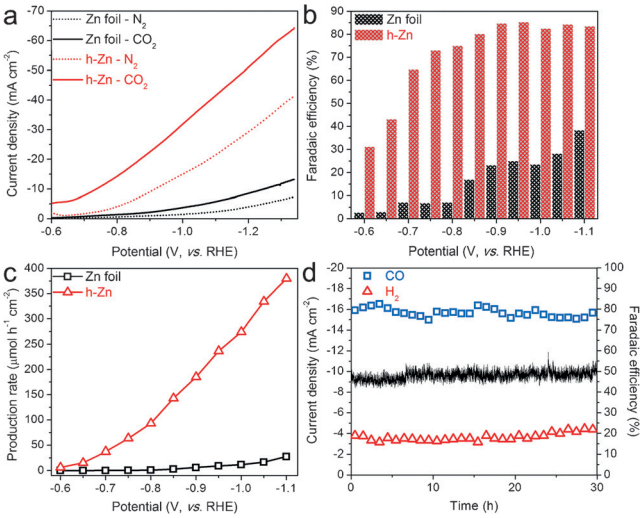


***Figure 2.*** a) LSV results in a $N_2$ (dotted line) or $CO_2$-saturated (solid line) 0.5 M $KHCO_3$ electrolyte with a 50 $mV s^{-1}$ scan rate. b) FE and c) production rates of CO at various constant potentials ranging from −0.6 to −1.1 V. d) Stability of the *h*-Zn. Current density (line) and FE (dot) of the *h*-Zn during 30 h of long-time operations at −0.85 V.

towards $CO_2$ reduction (Figure 2a). In a $CO_2$-saturated electrolyte, the reductive current densities from the *h*-Zn were about 9 times higher on average than those from the Zn foil over the entire potential range. The increased current density was mainly attributed to the enlarged surface area of the *h*-Zn, which could provide numerous active sites for $CO_2$ reductions.

To investigate the final product and its selectivity from $CO_2$ reduction on the prepared electrodes, electrochemical $CO_2$ reductions were carried out at selected potential range from −0.6 to −1.1 V (vs. RHE) in a $CO_2$-saturated 0.5 M $KHCO_3$ electrolyte. These data were obtained by performing step-potential electrolysis with periodic quantification of the gaseous products by gas chromatography. The products from $CO_2$ electrolysis were CO and $H_2$ with net total Faradaic efficiency (FE) of 96.5 ± 4.2% (Tables S1–S2). As shown in Figure 2b, the FE of CO was increased as the applied potential decreased on both Zn electrodes. At the selected potentials, the FE of CO was significantly improved on the *h*-Zn compared to the Zn foil (note that the $H_2$ evolution reaction (HER), which is the competitive reaction of $CO_2$ reduction, was consequently decreased on the *h*-Zn). The highest FE for CO was 85.4% at −0.95 V on the *h*-Zn, which was 60.3% p higher than the value for the Zn foil. The *h*-Zn performance was compared with other previous state-of-the-art Zn based electrodes (Table S3). The FE for CO of the *h*-Zn surpassed those of other Zn electrodes under similar experimental condition. Moreover, because of the outstanding current density and the high FE, the *h*-Zn also demonstrated a superior production rate of CO compared to other Zn electrodes (Figure 2c).

We then examined the performance profile of the *h*-Zn during long-term operation by collecting the current density and FE at −0.85 V (Figure 2d). The *h*-Zn exhibited stable operation over 30 h of electrolysis without significant performance degradation: the FE for CO was preserved as 80% maintaining $-9.5\ mA\,cm^{-2}$ of the current density. This result is of particular importance since no previous study reports CO production catalyst with durability over 12 h, to our knowledge; thus, the *h*-Zn demonstrated an unprecedented prolonged stability compared not only to the Zn-based catalysts, but even also to the noble metal catalysts (Table S4).

Although the selectivity of our *h*-Zn is already superior to that of other reported Zn-based catalysts, it should be further optimized to compete with other noble metal catalysts. A recent report suggested that an introduction of $Cl^-$ ion in electrolyte can improve the reaction selectivity for CO because of the adsorbed $Cl^-$ ion on the electrode surface inhibiting HER.[2d,4b,5d,6] As such, we further optimized the selectivity of our *h*-Zn by using a $CO_2$-saturated 0.5 M KCl electrolyte (Figure 3a and Table S5). This increased the FE of CO on the *h*-Zn up to about 95% despite of the sacrifice of the current density, which is comparable to those of noble metal catalysts. We also confirmed that the high selectivity obtained from the *h*-Zn in presence of $Cl^-$ can be maintained during 30 h of operation (Figure 3b).

Interestingly, the partial current densities of CO production on the *h*-Zn were 60-fold higher on average than those of the Zn foil, whereas the geometric surface area of the *h*-Zn

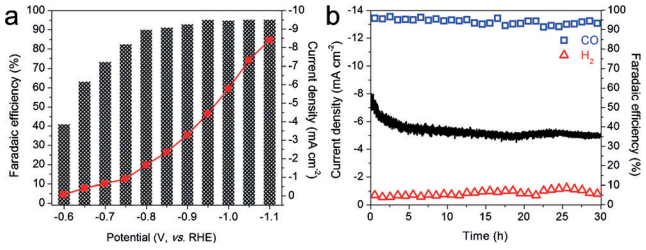


***Figure 3.*** Optimized CO selectivity by introduction of $Cl^-$ ion. a) FE of CO (bar) and current densities (square) at various constant potentials ranging from −0.6 to −1.1 V obtained in a $CO_2$-saturated 0.5 M KCl electrolyte. b) Stability of the *h*-Zn in KCl solution. Current density (line) and FE (dot) of the *h*-Zn during 30 h of long-time operations at −1.05 V.

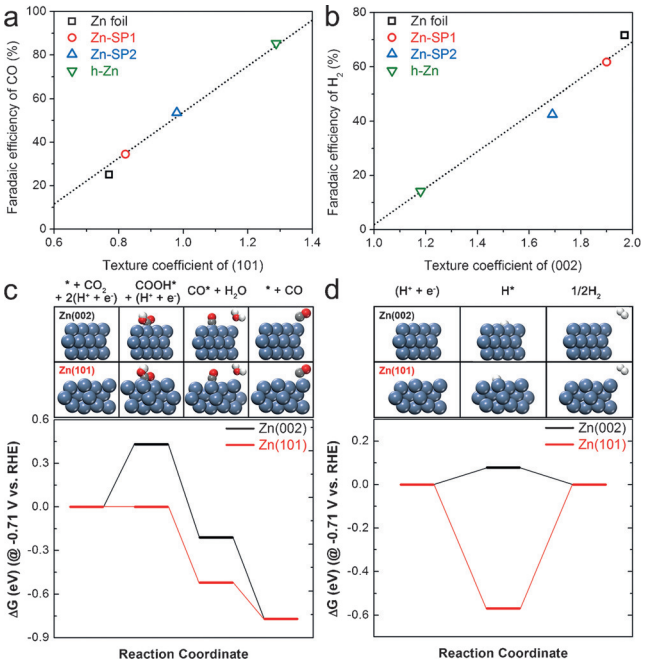


***Figure 4.*** Correlation curves between texture coefficient and FE of a) CO and b) $H_2$ at −0.95 V. Free-energy diagrams for c) $CO_2$ reduction and d) HER on Zn (002) (black solid line) or Zn (101) (red solid line) at −0.71 V. Atomistic structures optimized for each step are shown in the top. Navy blue, gray, red, and white colors represent Zn, C, O, and H atoms, respectively.

was increased only 15.8 times. This implies that the intrinsic $CO_2$ reduction activity of the *h*-Zn was improved because of newly constructed structure formed during electrodeposition. From the relative intensities of XRD analyses in Figure S5 a, we noticed that the electrodeposition procedure led our *h*-Zn to preferentially develop (101) facet (a pyramidal plane), while (002) facet (a smooth basal plane) was preferentially developed in the conventional Zn foil. By including two additional Zn electrodes with different crystal structures as control groups, namely Zn-SP1 and Zn-SP2, which were prepared by RF sputtering, we calculated texture coefficient of each (*hkl*) facet for the four different Zn-based electrodes (Zn foil, Zn-SP1, Zn-SP2, and *h*-Zn; Figure S5 b), and compared their catalytic selectivity (Figure S6 and Tables S6, S7). As shown in Figure 4 a,b, the texture coefficient of (101) facet showed a good positive correlation with the FE of CO ($R^2 = 0.99$), while the texture coefficient of (002) facet showed a good positive correlation with the FE of $H_2$ ($R^2 = 0.97$), both of which were measured at −0.95 V. We further confirmed that the observed strong correlation was preserved for all potential ranges (Figure S7), which suggests that (101) facet of Zn electrode is favorable to $CO_2$ reduction whereas (002) facet is favorable to HER.

To elucidate the origin of different catalytic selectivity derived from the Zn facets, we conducted DFT calculations for $CO_2$ reduction on (002) and (101) facets of Zn. For the electrochemical reduction of $CO_2$ to CO, three elementary reaction steps were considered as given in Equations (1)–(3),[7]

$$CO_2\ (aq) + [H^+ + e^-] \rightarrow COOH^*\ (aq) \quad (1)$$

$$COOH^*\ (aq) + [H^+ + e^-] \rightarrow CO^*\ (aq) + H_2O(aq) \quad (2)$$

$$CO^*\ (aq) \rightarrow CO\ (g) \quad (3)$$

where an asterisk (*) indicates an adsorbed species and the computational hydrogen electrode method was used for the chemical potential of proton and electron pair ($H^+ + e^-$).[8] Free energy diagrams for $CO_2$ reduction to CO are shown in Figure 4 c. The smooth Zn surface, (002) facet, shows high reduction potential of −1.14 V for $CO_2$ reduction. In case of rough Zn surface, (101) facet, however, the reduction potential is drastically decreased to −0.71 V. The lower reduction potential on (101) facet originates from its stronger ability to adsorb COOH molecule since the protonation of $CO_2$ generating the adsorbed •COOH is the reaction limiting step in both cases. This corresponds well to the aforementioned correlation between Zn facets and $CO_2$ reduction activities. The calculated free energetics for HER further convinced our contention, providing a better understanding on the different HER activity of the Zn facets (Figure 4 d). In contrast to the case of $CO_2$ reduction, the (002) facet requires low energy barrier of 0.08 eV during the first ($H^+ + e^-$) transfer step to Zn surface whereas the rough Zn facet (101) requires high energy barrier of 0.57 eV during the second ($H^+ + e^-$) transfer to produce $H_2$ at the same reduction potential of −0.71 V. Therefore, the outstanding performance of the *h*-Zn is clearly explained by its highly developed (101) facets, which require relatively low $CO_2$ reduction potential and high HER potential, as well as by its large surface area providing more active sites for $CO_2$ reduction. Based on the DFT results, we envisage that the catalytic performance of Zn electrode can be further enhanced by synthesizing Zn crystal with more (101) facets. Furthermore, the product distribution of CO/$H_2$ can be controlled by engineering a crystal plane ratio on Zn electrode (Figure S7 c), and this suggests that the tailored catalyst design for different industrial processes becomes feasible.

In summary, we developed the *h*-Zn, which selectively catalyzed the $CO_2$ reduction to CO with a high activity (379.9 μmol $h^{-1}$ $cm^{-2}$ at −1.1 V) and a selectivity (85.4 % without KCl, and 95.4 % with KCl in electrolyte) as well as

  

extremely high stability over 30 h. Significantly, we found that its high selectivity towards CO is correlated with the rough Zn facet (101). In particular, DFT calculations demonstrated that (101) facet is appropriate to CO production due to its lower reduction potential for $CO_2$ reduction to CO and higher energy barrier for HER than (002) facet. Because of a superior production rate of CO and a prolonged stability as well as a simple synthesis method, we anticipate that the *h*-Zn can be a promising catalyst for practical application in $CO_2$ reduction. Furthermore, we propose that manipulating the Zn crystal structure and its ratio can be used as a key control factor for product selectivity, and this study may suggest a design principle for further developments in other advanced catalysts as well as in $CO_2$ reduction.

## Acknowledgements

This research is supported by BK21PLUS program through the National Research Foundation (NRF) and the Global Frontier R&D Program on Center for Hybrid Interface Materials (HIM) funded by the Ministry of Science, ICT & Future Planning (grant number 2013M3A6B1078884).

**Keywords:** carbon dioxide · carbon monoxide · density functional calculations · electrocatalysis · zinc

**How to cite:** *Angew. Chem. Int. Ed.* **2016**, *55*, 9297–9300
*Angew. Chem.* **2016**, *128*, 9443–9446

[1] a) G. A. Olah, G. K. S. Prakash, A. Goeppert, *J. Am. Chem. Soc.* **2011**, *133*, 12881–12898; b) G. Centi, E. A. Quadrelli, S. Perathoner, *Energy Environ. Sci.* **2013**, *6*, 1711–1731.

[2] a) B. A. Rosen, A. Salehi-Khojin, M. R. Thorson, W. Zhu, D. T. Whipple, P. J. A. Kenis, R. I. Masel, *Science* **2011**, *334*, 643–644; b) T. Hatsukade, K. P. Kuhl, E. R. Cave, D. N. Abram, T. F. Jaramillo, *Phys. Chem. Chem. Phys.* **2014**, *16*, 13814–13819; c) A. Salehi-Khojin, H.-R. M. Jhong, B. A. Rosen, W. Zhu, S. Ma, P. J. A. Kenis, R. I. Masel, *J. Phys. Chem. C* **2012**, *116*, 1627–1632; d) Y.-C. Hsieh, S. D. Senanayake, Y. Zhang, W. Xu, D. E. Polyansky, *ACS Catal.* **2015**, *5*, 5349–5356.

[3] a) K. P. Kuhl, T. Hatsukade, E. R. Cave, D. N. Abram, J. Kibsgaard, T. F. Jaramillo, *J. Am. Chem. Soc.* **2014**, *136*, 14107–14113; b) H. Mistry, R. Reske, Z. Zeng, Z.-J. Zhao, J. Greeley, P. Strasser, B. R. Cuenya, *J. Am. Chem. Soc.* **2014**, *136*, 16473–16476; c) W. Zhu, Y.-J. Zhang, H. Zhang, H. Lv, Q. Li, R. Michalsky, A. A. Peterson, S. Sun, *J. Am. Chem. Soc.* **2014**, *136*, 16132–16135; d) X. Feng, K. Jiang, S. Fan, M. W. Kanan, *J. Am. Chem. Soc.* **2015**, *137*, 4606–4609; e) Y. Chen, C. W. Li, M. W. Kanan, *J. Am. Chem. Soc.* **2012**, *134*, 19969–19972.

[4] a) J. Rosen, G. S. Hutchings, Q. Lu, R. V. Forest, A. Moore, F. Jiao, *ACS Catal.* **2015**, *5*, 4586–4591; b) F. Quan, D. Zhong, H. Song, F. Jia, L. Zhang, *J. Mater. Chem. A* **2015**, *3*, 16409–16413; c) Y. Hori, H. Wakebe, T. Tsukamoto, O. Koga, *Electrochim. Acta* **1994**, *39*, 1833–1839.

[5] a) F. S. Roberts, K. P. Kuhl, A. Nilsson, *Angew. Chem. Int. Ed.* **2015**, *54*, 5179–5182; *Angew. Chem.* **2015**, *127*, 5268–5271; b) W. Tang, A. A. Peterson, A. S. Varela, Z. P. Jovanov, L. Bech, W. J. Durand, S. Dahl, J. K. Norskov, I. Chorkendorff, *Phys. Chem. Chem. Phys.* **2012**, *14*, 76–81; c) R. Reske, H. Mistry, F. Behafarid, B. Roldan Cuenya, P. Strasser, *J. Am. Chem. Soc.* **2014**, *136*, 6978–6986; d) A. S. Varela, W. Ju, T. Reier, P. Strasser, *ACS Catal.* **2016**, *6*, 2136–2144; e) M. F. Baruch, J. E. Pander, J. L. White, A. B. Bocarsly, *ACS Catal.* **2015**, *5*, 3148–3156; f) S. Zhang, P. Kang, T. J. Meyer, *J. Am. Chem. Soc.* **2014**, *136*, 1734–1737; g) D. Gao, H. Zhou, J. Wang, S. Miao, F. Yang, G. Wang, J. Wang, X. Bao, *J. Am. Chem. Soc.* **2015**, *137*, 4288–4291; h) D. H. Won, C. H. Choi, J. Chung, M. W. Chung, E.-H. Kim, S. I. Woo, *ChemSusChem* **2015**, *8*, 3092–3098; i) J. Chung, D. H. Won, J. Koh, E.-H. Kim, S. I. Woo, *Phys. Chem. Chem. Phys.* **2016**, *18*, 6252–6258.

[6] I. T. McCrum, S. A. Akhade, M. J. Janik, *Electrochim. Acta* **2015**, *173*, 302–309.

[7] H.-K. Lim, H. Shin, W. A. Goddard, Y. J. Hwang, B. K. Min, H. Kim, *J. Am. Chem. Soc.* **2014**, *136*, 11355–11361.

[8] J. K. Nørskov, J. Rossmeisl, A. Logadottir, L. Lindqvist, J. R. Kitchin, T. Bligaard, H. Jónsson, *J. Phys. Chem. B* **2004**, *108*, 17886–17892.

Received: March 23, 2016
Published online: June 28, 2016

  